Chapter 1
Introduction

For many years, lasers had been considered by engineers to be a problem in search of a solution—not the other way 'round, as is often repeated in the scientific literature. The problem was getting the laser to work properly, reliably, cost-effectively, etc.—and then getting it to "play" well with the other components in the system. This historical difficulty in obtaining working hardware with these unique sources of photons led to the many Immutable Laws of Lasers:

- The optimum number of lasers in any system is zero.
- The only likely result of a laser development program is that all available funds will be expended.
- The performance of any given laser cannot be predicted based on the measurements of the performance of any other laser.
- Lasers are the wave of the future—and always will be!

Fortunately, these laws have mutated over the years to the point where they are now mostly obsolete, and lasers are used in a number of difficult environments ranging from the manufacturing floor to the ceiling of outer space. Examples vary from the obvious to the obscure, including:

- Driverless cars and autonomous vehicles[1]
- Biomedical microscopes with sub-diffraction-limited resolving power, resulting in a Nobel prize for its inventors[2]
- The Internet and laser communications[3]
- Manufacturing applications requiring material heating, removal, or addition[4]
- Laser projection systems and displays[5]
- Directed energy (aka "Star Wars") for planetary defense against asteroids[6]

Despite their many applications—and the prominence of lasers in popular culture as well[7]—there is still a surprising lack of information available on how to design and engineer a laser *system*. The development

of lasers themselves has for years dominated academic research, yet the money has not flowed to the broader issues and intricacies involved in using these high-tech "flashlights" in industrial, commercial, biomedical, or defense applications. The purpose of this book is to take an initial step in filling this gap.

A laser is a source of both light and heat. Light is an electromagnetic wave with a wavelength λ and frequency ν with energy propagating at the speed of light c in vacuum:

$$\nu = \frac{c}{\lambda} \qquad [\text{Hz}] \tag{1.1}$$

The wavelengths that correspond specifically to "light" are shown in Fig. 1.1 as ultraviolet (UV), visible (VIS), and infrared (IR). The different types of lasers reviewed in this book can emit in any or all of these wavelength bands. Table 1.1 divides these bands into smaller units such as vacuum UV (VUV), midwave IR (MWIR), and so on.

In this chapter, we give an overview of the book by first looking in more detail at some laser systems that illustrate important laser properties (Section 1.1). As these properties depend on the design of the lasers themselves,

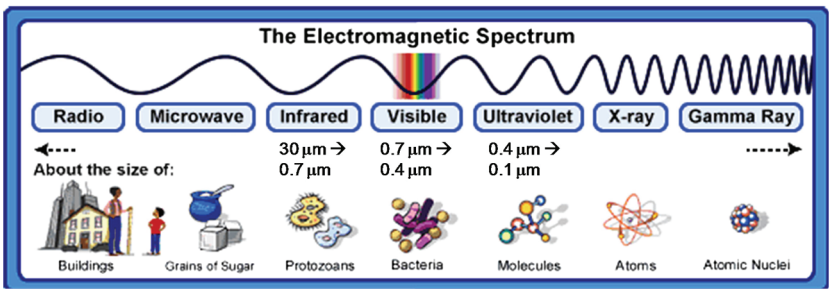

Figure 1.1 Optical electromagnetic wavelengths ("light") can be divided into infrared, visible, and ultraviolet bands. [Credit: NASA (www.nasa.gov)]. (See color plate.)

Table 1.1 Laser wavelength bands from Fig. 1.1 can be subdivided into near ultraviolet (NUV), near infrared (NIR), and so on.

Wavelength Band	Abbreviation	Wavelength (μm)
Vacuum ultraviolet	VUV	0.1–0.18
Deep ultraviolet	DUV	0.18–0.32
Near ultraviolet	NUV	0.32–0.40
Visible	VIS	0.4–0.7
Near infrared	NIR	0.7–1.0
Shortwave infrared	SWIR	1–3
Midwave infrared	MWIR	3–5
Longwave infrared	LWIR	8–12
Very longwave infrared	VLWIR	12–30

we then review in Section 1.2 the principles of laser engineering. Finally, we preview the book contents in Section 1.3 with an overview of the components used in typical laser systems, and some of the design trades required for optimizing overall laser system performance.

1.1 Laser Systems

As illustrated in Fig. 1.2, a generic laser system consists of lasers, optics, scanners, detectors, and a propagation medium such as air. As a result, the required tasks for laser system development may include laser selection, beam propagation, optical design, beam scanning, radiometry, detector selection, and possibly atmospheric compensation.

The heart of the laser system is, of course, the laser—of which there are nearly an infinite number of types and wavelengths (Fig. 1.3). One of the goals of this book is to narrow down the number of options to those that will cover 90% or so of the possible systems, with the more-obscure 10% not included. Some common laser systems—and the critical laser properties that make them useful—are reviewed in the rest of this section.

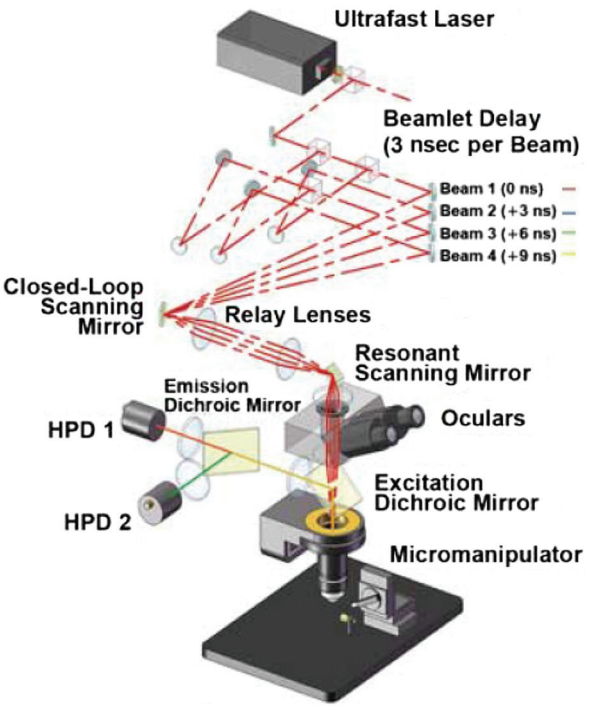

Figure 1.2 Typical laser system components include lasers, optics, scanners, and detectors. [Reprinted with permission from: A. Cheng et al., "Simultaneous two-photon calcium imaging at different depths with spatiotemporal multiplexing," *Nature Methods* **8**, 139–142 (2011).] (See color plate.)

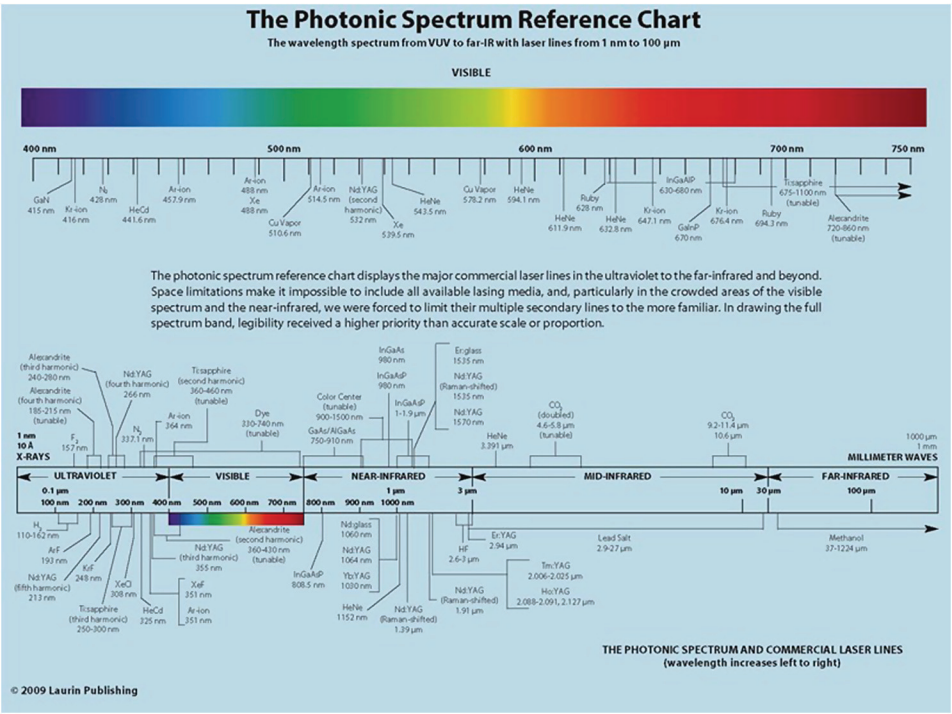

Figure 1.3 The large number of laser types and wavelengths makes laser selection for system development a complex task. (© 2009 Laurin Publishing; reprinted with permission.) (See color plate.)

The first system is that of optical data storage (Fig. 1.4) such as CD, DVD, and HD-DVD players, and holographic data storage. In this case, low-power semiconductor diode lasers are commonly used because a property known as *beam quality* (Chapter 3) allows focusing to the smallest possible, diffraction-limited spot size ($\sim \lambda/D$ for an objective lens with an aperture diameter D). This ensures the highest possible storage capacity on the limited surface area of a disk; a shorter wavelength also increases capacity, with wavelengths evolving from $\lambda = 780$ nm for CD systems down to 405 nm for HD-DVDs such as Blu-ray™. Additional benefits of diode lasers—critical for the consumer market—include their low cost, size, and electrical power consumption.

Another common laser application is that of testing the irregularity of optical surfaces.[8] Such testing requires a laser with a large coherence length, i.e., the distance over which its phase is approximately unchanged (Section 1.2.1). For example, the laser's coherence length must exceed twice the distance between the reference surface and the test surface in Fig. 1.5, as any difference in phase will interfere and appear incorrectly as an error in the surface of the test mirror. Helium-neon (HeNe) gas lasers are often used for interferometers because they have both a long coherence length and good

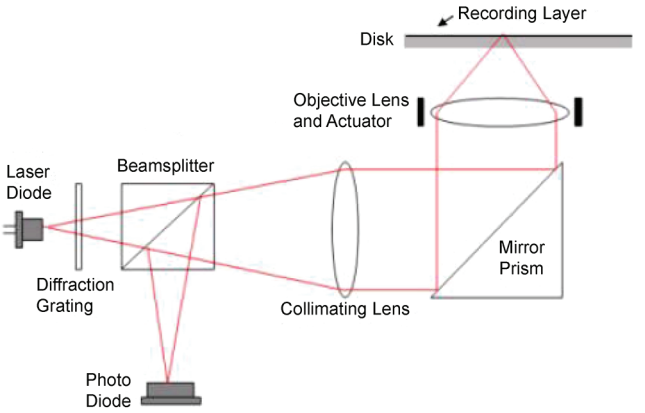

Figure 1.4 Optical data storage requires lasers with beams that can be focused to the smallest possible spot size. [Reprinted from W.-S. Sun et al., "Compact HD-DVD pickup head with a lens-prism," *Proc. SPIE* **5174**, 128–135 (2003).] (See color plate.)

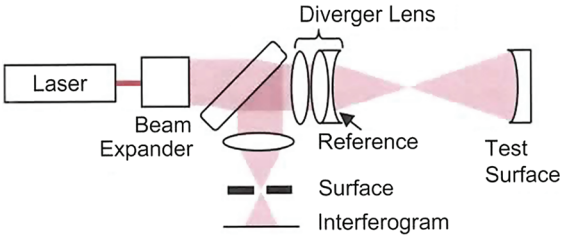

Figure 1.5 A Fizeau interferometer used for testing optical surfaces requires the long coherence length of a laser. (Reprinted with permission from Ref. 8, p. 59.)

spatial coherence across the wavefront. Helium-neon wavelengths of 633 nm (VIS) and 3.39 μm (MWIR) are common, as are carbon dioxide (CO_2) gas lasers with a wavelength of 10.6 μm for testing LWIR optics.

A third laser application is that of directed energy (DE), where it is necessary to deposit the highest amount of power in the smallest area at a large distance. This places a requirement on the laser brightness; distinct from simply output power, laser brightness is a measure of how spatially efficient a source is at emitting power. For example, if the output power of two lasers is the same, the laser emitting with fewer atoms (a smaller area) into a smaller divergence angle has a higher brightness (Chapter 6). Solid-state and fiber lasers can deliver more than 10 kW of average power from a small, near-diffraction-limited beam and are thus an option for DE applications requiring high irradiance (W/cm^2) or fluence (J/cm^2) on a target.

Finally, a fourth common laser application is that of confocal microscopy. As illustrated in Fig. 1.6, these microscopes obtain high-resolution 3D images

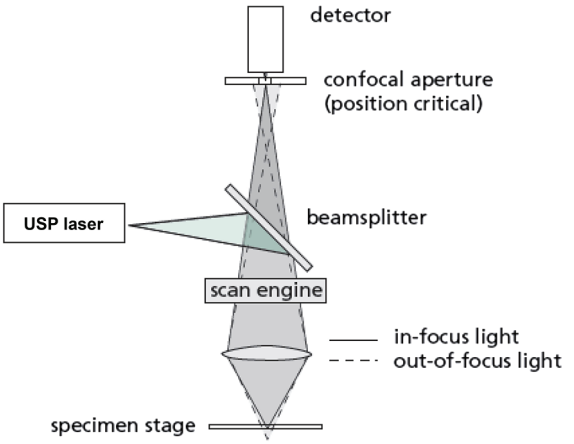

Figure 1.6 MPE confocal microscopy relies on ultrashort-pulse (USP) lasers with high peak power and low average power. (Credit: CVI Laser, LLC.)

by blocking out-of-focus photons with a detector pinhole (confocal aperture). Using a technique known as multiphoton excitation (MPE), image contrast can be improved by using a low-average-power laser that creates one short-λ photon from two (or more) longer-λ photons. The key laser properties that allow MPE are a high peak power (to efficiently generate long-λ photons) and low average power (to minimize heat absorption by the specimen). This requires ultrashort-pulse (USP) lasers that can release energy in a short pulse or "shot" on the order of 1–10 psec (Section 2.1.5). Fiber lasers allow the generation of such pulses in a product size appropriate for clinical use.

Summarizing, we see that various laser properties—beam quality, coherence length, brightness, pulse width, and so on—may or may not be important depending on the application. There are, of course, many other laser systems besides the four discussed in this section (see Table 1.2), and we will look at a number of these throughout the course of the book. As well, the different types of lasers—semiconductor, gas, solid-state, and fiber—and their properties will be reviewed in more detail in Chapter 2.

1.2 Laser Engineering

While the intent of this book is to go into detail on the development of laser systems, a brief introduction to the design of lasers themselves makes their use in a system a more-intelligent endeavor. Many references are available for details on laser design; Ref. 9 is recommended.

One of the primary goals of laser engineering is to meet system requirements by controlling the unique features of lasers that determine the properties of coherence length and beam quality, namely, the degree of

Table 1.2 Critical system properties (or key performance parameters) required for various laser applications. The laser types and properties will be reviewed in detail in Chapter 2.

Laser Application	Wavelength and Laser Type	Key Performance Parameters (KPPs)
HD-DVD Players	405 nm; diode	Spot size, size, cost
Bar-Code Scanners	670 nm; diode	Size, cost
Laser Communications	1550 nm; diode	Modulation rate, noise
Fluorescence Microscopy	400–1100 nm; multiple	Spot size, peak power
Eye Surgery ("LASIK")	193 nm; excimer	Spot size, power stability
Precision Manufacturing	0.3–10.6 μm; multiple	Spot size, peak power, PRF
Interferometry	633 nm, 3.39 μm; gas	Coherence
Semiconductor Lithography	193 nm; excimer	Spot size, energy stability
Laser Pumping	808, 980 nm; diode	Wavelength, power
Laser Rangefinder	1.55 μm; solid-state	Peak power, beam quality
Laser Radar	1.064 μm; solid-state	Peak power, beam quality
Directed Energy	1 μm; solid-state, fiber	Brightness, efficiency
IR Countermeasures	3-5 μm; QCL	Wavelength, brightness

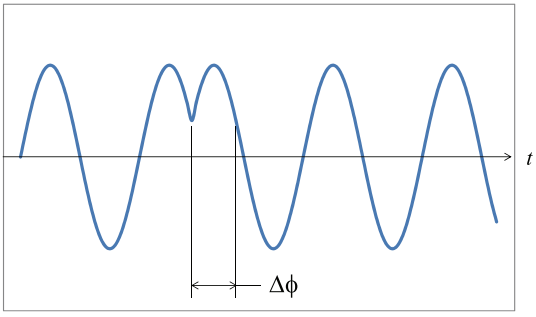

Figure 1.7 Collisions between gas molecules create temporal phase jumps $\Delta\phi$ in their emitted wavefronts, affecting the propagating frequencies and the laser's temporal coherence.

phase coherence. That is, the wavefronts must be in phase along the propagation direction (temporal coherence, Fig. 1.7); in addition, the wavefronts must also be in phase across the beam diameter (spatial coherence, Fig. 1.8). There are also variations on these themes, where specialized lasers have low temporal coherence but good spatial coherence (white-light or super-continuum lasers), or high temporal coherence but poor spatial coherence ("random" lasers).

As shown in Fig. 1.9, what's needed for a laser's temporal and spatial coherence is:

- A gain medium (and associated pump energy $h\nu_p$) to create a population inversion (or gain) of the medium's electron energy states [Fig. 1.9(a)], allowing photon amplification.

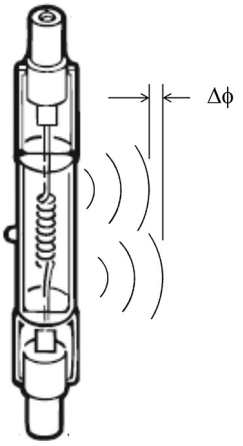

Figure 1.8 Atoms emitting independently across an incoherent source such as a tungsten-filament lamp results in a phase difference $\Delta\phi$ and poor spatial coherence of the wavefronts. (Permission to reprint granted by Newport Corporation; all rights reserved.)

- A resonant cavity—two mirrors, for example—to control the number, direction, and phase coherence of the amplified photons [Fig. 1.9(b)].

The amplification of photons is in phase with the incident wavefront and is known as stimulated emission, while atoms that spontaneously emit photons before they interact with the laser beam have a random phase relationship (i.e., are not coherent) with the wavefront (Fig. 1.10). As a result, higher gain has a larger fraction of amplified in-phase photons in comparison with the incoherent photons.

If the energy of the incident electromagnetic field more-or-less matches that of the electron's excited state energy E_2 compared with some lower-energy state

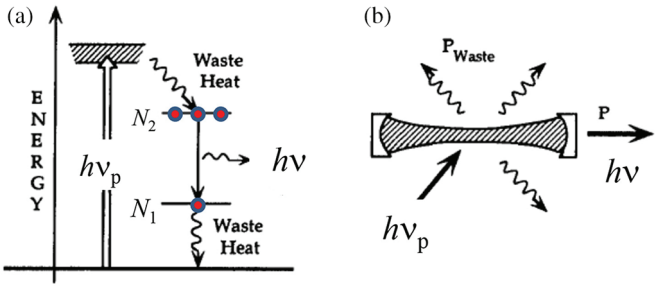

Figure 1.9 (a) Changes in the gain medium's electron energy states result in the emission of a photon with energy $h\nu$. (b) The back-and-forth reflections in a two-mirror resonant cavity increase the number of stimulated photons. (Reprinted from Ref. 10.)

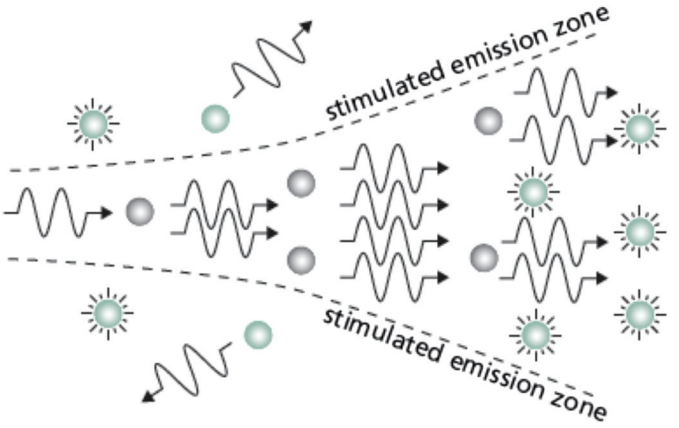

Figure 1.10 The wavefronts of stimulated photons are emitted in phase with the incident photons. (Credit: CVI Laser, LLC.)

E_1, then there is a high probability the electron will give up its energy in the form of a stimulated photon whose energy E_p in Fig. 1.9(a) is

$$E_p = E_2 - E_1 = h\nu = \frac{hc}{\lambda} \qquad [J] \tag{1.2}$$

where $h = 6.626 \times 10^{-34}$ J-sec is Planck's constant. Physically, a higher-frequency, shorter-wavelength photon has more energy, as would be expected for an electromagnetic wave that changes at a faster rate.

The population inversion—defined as $N_2 - N_1$ in Fig. 1.9(a), with more electrons in the gain medium in an excited energy state E_2 than a lower state E_1—has a distribution of excited-state energies and thus amplifies more than a single wavelength. In its simplest form, this distribution is a result of the inevitable Heisenberg uncertainty fluctuations of the excited-state lifetime, resulting in a spread of photon energy $\Delta E_p = h\Delta\nu$ that is known as the *gain bandwidth* (in units of energy).

Building on these principles, laser engineering entails a large number of complexities, some of which are reviewed in the next subsections under the categories of temporal coherence, spatial coherence, pulse generation, and wavelength conversion.

1.2.1 Temporal coherence

We have seen in Section 1.1 how the coherence length affects the performance of an interferometer; in this section, we take another look at this idea from the laser designer's perspective.

Even though it is common to talk of a pure "red" or 633-nm wavelength, no laser emits at a single (monochromatic) wavelength. Instead, there are unavoidable gain medium, quantum-mechanical, and optomechanical

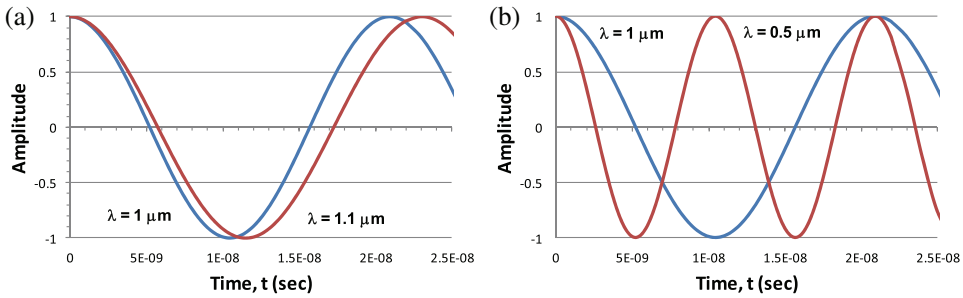

Figure 1.11 Coherence length $d_c = c\tau_c$ is the distance over which different wavelengths become out of phase, with (a) a smaller $\Delta\lambda$ giving a longer coherence length, and (b) a larger $\Delta\lambda$ giving a shorter coherence length.

broadenings of any laser's wavelength, and the degree of broadening—or *linewidth* $\Delta\lambda$—determines the laser's temporal coherence and coherence length.

Temporal coherence can be understood by using a physical picture of two wavelengths propagating along the laser's longitudinal axis. Even if the speed of light is the same for both wavelengths, Fig. 1.11 shows that they will eventually get completely out of phase. The distance over which this occurs is known as the coherence length d_c.

The coherence time τ_c over which the emitted wavelengths are considered to be in phase—that is, are temporally coherent—thus depends inversely on the absolute value of the wavelength difference $|\Delta\lambda|$ or frequency difference $\Delta\nu = c|\Delta\lambda|/\lambda^2$ [from differentiating Eq. (1.1)]:

$$\tau_c \approx \frac{1}{2|\Delta\nu|} = \frac{1}{2c}\frac{\lambda_o^2}{|\Delta\lambda|} \qquad [\text{sec}] \tag{1.3}$$

clearly showing that a narrow-spectrum laser with small $\Delta\nu$ has a longer time over which different frequencies propagate before they are no longer considered to be in phase. Typical numbers for a HeNe laser used for interferometeric optical testing are a coherence time $\tau_c = 0.33$ nsec and a coherence length $d_c = c\tau_c = 100$ mm for a linewidth $\Delta\lambda = 2$ pm (see Table 1.3). Note that the results shown in Fig. 1.11(b)—where the different wavelengths

Table 1.3 Coherence length $d_c = c\tau_c$ of commonly used lasers; see Chapter 2 for more detail on each of these laser types.

Laser Type	Center Wavelength, λ_o	Linewidth, $\Delta\lambda$ or $\Delta\nu$	Coherence Length, d_c
High-Power Diode	808 nm	3 nm	100 μm
Nd:YAG	1064 nm	50 pm	10 mm
He-Ne	633 nm	2 pm	100 mm
Low-Power Fiber	1070 nm	10 kHz	15 km

are out of phase at a time $t \approx 10^{-8}$ sec—are not consistent with the estimates from Eq. (1.3), as the equation assumes that $\Delta\lambda$ is small in comparison with the center wavelength λ_o.

What determines the lasing wavelength λ_o and linewidth $\Delta\lambda$? Ideally, three factors: the axial modes based on the length of the laser cavity, the bandwidth of the gain medium, and the type of gain medium (homogeneous versus inhomogeneous).

Axial (or longitudinal) modes are determined by the geometrical fit (or *resonance*) of a given wavelength in the laser cavity. That is, if the two mirrors that define a laser cavity are nearly planar and perfectly reflecting—an ideal assumption, given that one mirror will be designed *not* to be so that light can escape the cavity as output power—then Fig. 1.12 shows that an integer number $m = 1, 2, 3$, etc., of half-wavelengths of the electric field fit in the cavity length L:

$$m\frac{\lambda}{2n} = L \qquad [\text{m}] \tag{1.4}$$

where the refractive index n of the gain medium is included to account for the reduction in wavelength in comparison with its free-space ($n = 1$) value. With the exception of a specific type of semiconductor laser known as a vertical-cavity surface-emitting laser (VCSEL) with a cavity length $L \approx \lambda$, the number of half-wavelengths is large in practice. For example, for a HeNe laser emitting at $\lambda = 633$ nm with $L = 100$ mm and $n \approx 1$, $m = 2L/\lambda = 2 \times 0.1$ m/633 nm = 315,955 half-wavelengths.

Unless they are specifically "locked" together in phase (as in Section 1.2.3), these axial modes are emitting independently of one another, and are thus all potential wavelengths at which the laser can oscillate. Solid-state lasers using titanium-doped sapphire as a gain medium, for example, may emit hundreds of thousands of axial-mode wavelengths (Section 2.2.2). These lasers are commonly specified by the frequency difference between each axial mode,

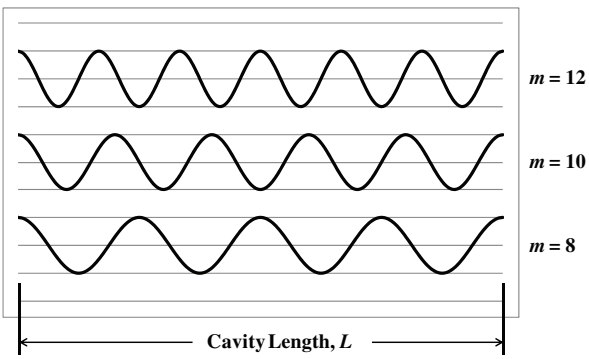

Figure 1.12 An integer number m of half-wavelengths ($m\lambda/2n$) of the electric field fit inside a perfectly reflecting resonant cavity, a simplifying assumption used to describe axial modes.

where each frequency ν_m for a planar cavity is obtained by combining Eqs. (1.1) and (1.4),

$$\nu_m = \frac{c}{\lambda_m} = \frac{mc}{2nL} \qquad [\text{Hz}] \tag{1.5}$$

and the frequency difference $\Delta\nu_a$ between adjacent axial modes—also known as the free spectral range (FSR) of the laser cavity—is given by

$$\Delta\nu_a = \nu_{m+1} - \nu_m = \frac{c}{2nL} \qquad [\text{Hz}] \tag{1.6}$$

For example, a HeNe laser with $L = 100$ mm has an axial mode spacing $\Delta\nu_a = (3 \times 10^8 \text{ m/sec})/(2 \times 1 \times 0.1 \text{ m}) = 1.5$ GHz, while a short-cavity semiconductor laser with $L = 100$ μm and $n = 3$ gives $\Delta\nu_a = (3 \times 10^8 \text{ m/sec})/(2 \times 3 \times 100 \times 10^{-6} \text{ m}) = 500$ GHz.

Whether or not multiple axial modes will lase depends, in part, on the cavity-mode spacing $\Delta\nu_a$ in comparison with the frequency spectrum (or gain bandwidth) $\Delta\nu_g$ of the gain medium. This is shown in Fig. 1.13, where the gain curve is superimposed over the longitudinal modes of an ion laser. The gain bandwidth is determined by a number of possible gain-medium mechanisms: natural broadening due to spontaneous decay of excited-state energies, Doppler broadening due to atomic or molecular motion, collision broadening due to intermolecular impacts of gas molecules that change the phase of the emitted wavefront (Fig. 1.7), or phonon broadening due to imperfections and variations in lattice spacings in semiconductor, solid-state and fiber lasers. Independent of mechanism, a gain bandwidth wider than the axial mode spacing—as shown in Fig. 1.13—has the potential to lase at more than one axial-mode wavelength.

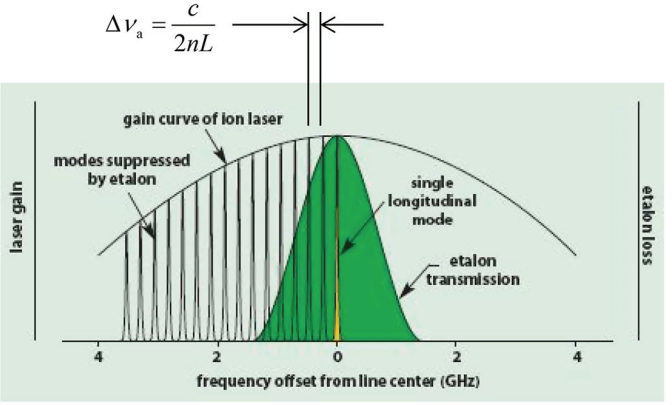

Figure 1.13 The gain bandwidth $\Delta\nu_g$ of many lasers exceeds the longitudinal-mode spacing $\Delta\nu_a$. (Permission to reprint granted by Newport Corporation; all rights reserved.)

Whether or not this occurs depends on the third contributor to the emission wavelength and linewidth, namely, how the gain medium responds (saturates) to power levels inside the cavity. There are two possibilities: (1) the gain decreases equally across the entire gain bandwidth as excited-state population levels are used up to increase the output power (homogeneous saturation), or (2) the gain decreases only at specific wavelengths depending on the gain-broadening mechanism (inhomogeneous saturation).

For homogeneous gain saturation—as is found with natural, collision, and homogeneous phonon broadening—the peak of the gain at steady state will drop to equal the cavity losses, and this will occur at or near one axial mode. This mode will thus lase, and homogeneous saturation typically leads to single-longitudinal-mode (SLM) lasing at one axial mode (aka single-frequency), rather than over the entire gain curve.[11] Stimulated emission thus results in a narrowing of the output spectrum from its spontaneous width $\Delta\nu_g$, a principal reason for the narrow linewidth of a laser; as a result, semiconductor lasers have a smaller $\Delta\lambda$ than spontaneously emitting LEDs made from the same material.

For inhomogeneous saturation, on the other hand, the gain saturates only at those axial-mode wavelengths preferred by the gain medium—with Doppler and inhomogeneous (strained lattice) phonon broadening being typical examples. This can lead to lasing at more than one axial mode, and such multi-longitudinal-mode lasers emit at discrete frequency spacings given by Eq. (1.6).

For a long coherence length, then, the first option for the laser systems engineer is a frequency-stable SLM laser, as is required for interferometry, coherent sensing, and holography. Because the drop-off of the gain curve might not be sufficient to prevent small cavity and refractive-index fluctuations from causing the axial mode to "hop" to an adjacent wavelength, laser designers might also use an additional frequency-stabilization component in the cavity.

The most commonly used component is a Fabry–Pérot (FP) etalon. In its simplest form, this is a flat piece of glass whose thickness d_{FP} is much smaller than the laser cavity's, and its axial mode spacing is thus much larger [Eq. (1.6)]. As seen in Fig. 1.13—where only one axial mode of the etalon is shown—the wavelengths that can lase are now based on the superposition of the etalon transmission and the longitudinal modes of the laser. The full-width at half-maximum (FWHM) bandwidth $\Delta\nu_R$ of the etalon transmission is based on its finesse F_R and axial mode spacing $\Delta\nu_{FP} = c/2nd_{FP}$:

$$\Delta\nu_R = \frac{\Delta\nu_{FP}}{F_R} \approx \frac{c}{2nd_{FP}} \cdot \frac{1-\sqrt{R_{p1}R_{p2}}}{\pi(R_{p1}R_{p2})^{1/4}} = \frac{c}{2nd_{FP}} \cdot \frac{1-R}{\pi\sqrt{R}} \qquad \text{[Hz]} \qquad (1.7)$$

for surface power reflectivities R_{p1} and R_{p2}, valid for $R \equiv (R_{p1}R_{p2})^{1/2} \geq 0.4$ or so. The etalon's transmission bandwidth is usually much smaller than its mode spacing; e.g., using an etalon with $R = 0.9$ gives $F_R = \pi R^{1/2}/(1-R) \approx 30$.

Because the mode spacing of the etalon is so much larger than that of the laser, however, even a relatively wide $\Delta\nu_R$ may drop off faster with laser frequency than the gain curve (Fig. 1.13); as a result, the laser is less sensitive to small fluctuations in power, cavity length, or refractive index, and mode hops are less likely to occur. In practice, the etalon bandwidth also depends on the parallelism and flatness of its surfaces—effects that can be controlled to such a degree with the fabrication of the etalon as to still make the etalon a useful frequency-stabilization component.

Even a frequency-stabilized SLM laser has a linewidth—an unavoidable consequence of random spontaneous-emission phase variations resulting from quantum fluctuations in excited-state energy levels. For such lasers, the ideal single-mode (Schawlow–Townes) linewidth $\Delta\nu_{ST}$ for a laser cavity $\Delta\nu_R$ (not its etalon) is given by Refs 9 and 12 as

$$\Delta\nu_{ST} = \frac{\pi h\nu \cdot (2\pi\Delta\nu_R)^2}{P} \qquad [\text{Hz}] \tag{1.8}$$

where P is the output power of the given axial mode. Physically, the higher power has a larger fraction of amplified in-phase photons in comparison with the incoherent, out-of-phase photons from spontaneous emission, reducing $\Delta\nu_{ST}$ to something smaller than the cold-cavity FWHM bandwidth $\Delta\nu_R$ of the *laser's* axial modes [also Eq. (1.7)] given the laser-cavity reflectivity R.

Equation (1.8) represents the ultimate lower limit on linewidth, with no commercial products able to achieve this level of frequency stability (< 1 Hz). In practice, some SLM fiber lasers have a linewidth smaller than 10 kHz—limited by "technical noise" (fluctuations in optical and optomechanical parameters, e.g.), and resulting in a coherence length $d_c \geq 15$ km.

There are, of course, many applications where coherence length is either unimportant or a hindrance to system performance. One example is that of speckle, where the reflections from a rough surface coherently interfere to produce a spotted image—a huge disadvantage for laser-based displays. In such cases, the system might still be limited by a different property of importance to both laser designers and systems engineers, namely, spatial coherence.

1.2.2 Spatial coherence

We have mentioned in Section 1.1 how the concept of beam quality affects focused spot size for optical data storage; in this section, we take a closer look at this idea from the laser designer's perspective. We have also seen in Section 1.2.1 how the laser wavelength is determined by three factors, but in practice additional factors such as mode hopping play a role. In this section we will see that yet another factor—the spatial coherence—also affects the lasing wavelength.

As discussed by Siegman (Ref. 9, pp. 55–58), the concepts of spatial coherence and beam quality arise because there may be phase variations $\geq \lambda/4$ across the diameter of each mirror in any laser cavity. These variations can result from manufacturing imperfections in each mirror, refractive-index non-uniformities of the gain medium, or misalignments of the mirrors.[13]

A typical laser cavity for solid-state and gas lasers[14,15] is shown in Fig. 1.14. Known as a confocal resonator, this particular type of cavity is designed with the radius of curvature of each mirror (R_1 and R_2) centered on the surface of the opposing mirror one cavity length L away. In the absence of manufacturing imperfections and index non-uniformities, this cavity is relatively stable against misalignments and produces a beam with a Gaussian irradiance profile and has no phase variations across it. In addition, the electric and magnetic fields are transverse to the longitudinal axis, and the combined irradiance and phase profiles are known as a Gaussian beam, i.e., a spatially coherent transverse electro-magnetic (TEM_{00}) mode of order (0, 0).

In practice, unavoidable misalignments between mirrors are one of the most common causes of excessive phase variations across the beam (Fig. 1.15)—and resulting loss of beam quality. For a small misalignment angle $\Delta\theta$, which keeps the on-axis length L the same by pivoting around the mirror surface at the longitudinal (or z) axis, there is still an optical axis determined by the line connecting the center of curvature of each mirror. However, there is also the potential for an asymmetry in the phase of the wavefront if the optical axis propagates through a solid-state crystal or Brewster window at an angle (see Section 2.1.12). Such asymmetries—astigmatism and coma, for example—can also result from manufacturing imperfections in each mirror or refractive-index non-uniformities in the gain medium.

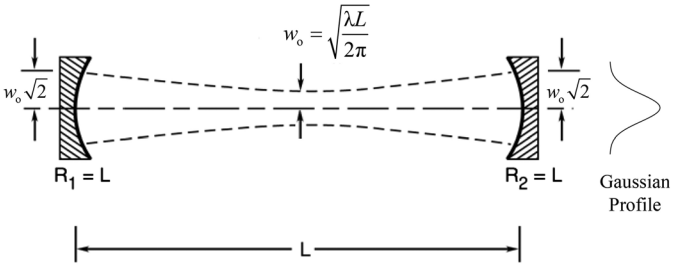

Figure 1.14 A symmetric confocal laser cavity with the radius of curvature of each mirror (R_1 and R_2) equal to the cavity length L. The minimum beam radius (or *waist*) w_o is at the center of the cavity where the focal length $f = R_i/2 = L/2$ of each mirror coincides. [Adapted from R. Scheps, *Introduction to Laser Diode-Pumped Solid State Lasers*, SPIE Press, Bellingham, Washington (2002).]

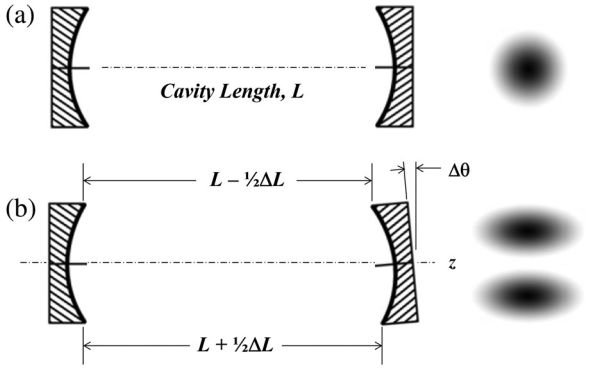

Figure 1.15 An angular misalignment $\Delta\theta$ can distort the Gaussian TEM_{00} profile in part (a), creating a phase difference across the beam and a lobed, circularly asymmetric irradiance profile in part (b) known as a TEM_{01} spatial mode. Higher- and multi-order spatial modes are also possible.

To first order, the asymmetries result in an approximate phase difference $\Delta\phi$ across the beam proportional to the change in cavity length ΔL at the edges of the mirrors:

$$\Delta\phi \propto \frac{2\pi n}{\lambda}\Delta L \qquad [\text{rad}] \tag{1.9}$$

where the type of mirror determines the actual phase difference. Two flat mirrors, for example, give $\Delta L = D\Delta\theta$, while curved mirrors will modify the phase with an additional quadratic term ($\Delta L = D^2/2R_i$) that depends on the diameter D and radius of curvature R_i of the mirrors.

As a Gaussian beam starts to develop from spontaneous emission within the cavity, there are additional phase terms—Gaussian wavefront propagation (see Chapter 3), Guoy phase shift, and so on—that become important with misaligned mirrors. Independent of these details, the phase variations across the mirrors modify the Gaussian beam in three ways: (1) an increase in the divergence angle at which the beam exits the laser; (2) an increase in spot size if the beam is focused with a lens; and (3) a small shift in the emission wavelength, and a possible linewidth broadening as well.

The beams that result can be either aberrated Gaussians (for small misalignments) or are no longer circularly symmetric, with the asymmetric profile of the misalignment direction [Fig. 1.15(b)] and one (or more) zero-irradiance lines (or *nodes*). The mode shown in Fig. 1.15(b), for example, is a TEM_{01} mode because there are no nodes in the horizontal direction and one node in the vertical. Depending on the degree of phase shift across the mirror, there might be higher-order modes as well, specified as TEM_{pq} for the integers $p > 0$ and $q > 0$ defining the number of nodes in the profile.

It sometimes happens that the transverse irradiance profile from a misaligned cavity is circularly symmetric, even though the profile shown in Fig. 1.15(b) is not. This occurs when the misalignments in both directions combine to produce a symmetric beam. A common example is the "donut" mode—a combination of TEM_{01} and TEM_{10} profiles—which is circularly symmetric. This is perhaps the most common multi-transverse-mode profile, as it is likely that there will be a slight angular misalignment of the cavity mirrors about both the x and y axes. In practice, it is unusual to obtain a pure higher-order mode such as TEM_{31}, as other contributors such as contamination or manufacturing imperfections of each mirror and refractive-index nonuniformities contribute to the phase profile, leading to combinations of modes.

Whether single- or multiple-spatial mode, the paraxial transverse irradiance distribution in free-space lasers is described mathematically by the product of the circularly symmetric Gaussian distribution and the Cartesian-coordinate Hermite polynomials.[9] Experimentally, the spatial-mode "content" is determined by a quantity known as M^2 which, as we will see in detail in Chapter 3, can be used to determine the increase in divergence angle and/or focused spot size. An ideal, diffraction-limited beam has an $M^2 = 1$; lasers with $M^2 \leq 1.5$ or so are said to have good beam quality.[16]

The third modification of a Gaussian beam that results from transverse spatial modes is a small shift in the emission wavelength, in addition to a possible linewidth broadening. This is shown in Fig. 1.16, where each longitudinal-mode frequency ν_m has transverse-mode frequencies associated with it. That is, the transverse modes—TEM_{01}, TEM_{11}, TEM_{12}, TEM_{22}, and so on—each have a slightly different frequency, given by

$$\nu_{pqm} = \frac{c}{2nL}\left[m + \frac{1}{\pi}(1+p+q)\cos^{-1}\sqrt{(1-L/R_1)(1-L/R_2)}\right] \quad \text{[Hz]} \quad (1.10)$$

where the $1 - L/R_i$ term is also referred to in the literature as a cavity stability parameter g_i.[9] In addition, the terms inside the square brackets in Eq. (1.10)

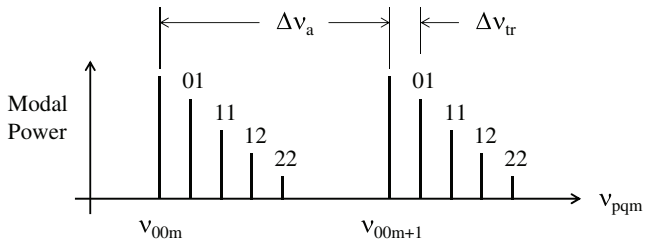

Figure 1.16 Transverse modes associated with a TEM_{00} axial mode have a frequency that differs from that of the axial, potentially leading to a broadening of the linewidth (and decrease in coherence length) for multi-spatial-mode lasers.

show that each Gaussian TEM_{00} mode may or may not have the same optical frequency as that given in Eq. (1.5) for a planar cavity.

As an example of the transverse-mode frequencies for a confocal cavity with $L = R_i$, we have $\cos^{-1}(0) = \pi/2$, giving $\nu_{00m} = (c/2nL) \times (m + ½)$ and $\nu_{01m} = (c/2nL) \times (m + 1)$. The transverse mode spacing $\Delta\nu_{tr}$ is then $\nu_{01m} - \nu_{00m} = c/4nL$, or one-half of the axial mode spacing $\Delta\nu_a$. Also note that the absolute value of the axial-mode frequency ν_{00m} has shifted to a higher frequency by the same amount, given the factor of $m + ½$ in comparison with the factor of m in Eq. (1.5) for a near-planar cavity [for which the $\cos^{-1}(1)$ term for $R_i \approx \infty$ is zero, reducing Eq. (1.10) to Eq. (1.5) for TEM_{00} modes].

There are other cavity designs—semi-confocal, spherical, hemispherical, etc.—where the transverse mode spacing is much smaller than that for the confocal cavity.[9] For designs that are relatively insensitive to misalignments—confocal and the widely used near-hemispherical (or half-concentric)—it is feasible to control the misalignments, fabrication errors, index non-uniformities, and mirror cleanliness to such a degree that single-spatial-mode lasers with near-TEM_{00} beam quality are common and inexpensive. These lasers will be reviewed in detail in Chapter 2.

In summary, beam quality is a measure of the phase variations across a beam.[16] The resulting transverse spatial mode properties—the systems-level consequences of which will be reviewed in Chapters 2 and 3—are an increase in beam divergence angle and focused spot size, as well as the possibility of a shift in wavelength in comparison with an ideal near-planar cavity. Also note that the term "multimode laser" can be ambiguous, as we have seen in this section that in addition to multi-longitudinal-mode lasers, there are also multi-transverse-modes that must be considered in system design. More typically, "multimode" refers to spatial modes, while "multifrequency" refers to axial modes.

1.2.3 Pulse generation

The lasers considered up to this point have been continuous wave (CW), with no obvious change in power level over time. In many applications, however, there is a need to concentrate the lasing energy into a shorter period of time—a pulse of width Δt_p—to increase the *peak* output power $P_{peak} = Q_p/\Delta t_p$ for a pulse energy Q_p (Section 2.1.4). As we will see, applications for which this is important include nonlinear wavelength conversion (Section 1.2.4), "cold" laser machining (Section 2.1.5), multiphoton microscopy, as well as laser ranging and active imaging where the detector responds to reflected peak power (Chapter 7).

The first and most obvious approach to generating pulses is to switch the pump (and thus the gain) on-and-off—resulting in pulse widths shorter than the pump pulse, but with low peak power.[9] This is a result of the dynamic interaction between excited-state electrons and photons leading to relaxation oscillations as the excited-state energies "relax" (and are stimulated) to a lower-energy state; reducing these oscillations limits the degree of

above-threshold pumping and thus the peak powers obtained. Despite its limitations, such gain switching is necessary for some types of CO_2 and excimer lasers for which other types of switching are not practical.

To avoid the relaxation oscillations and generate much higher peak power than is possible with gain switching, two methods are used for pulse generation: Q-switching and mode locking.

The concept of Q-switching refers to changing the quality Q_c of the laser cavity. "Quality" in this case is not the transverse beam quality, but the cavity's ability to store laser energy:

$$Q_c = 2\pi\nu_{pqm}\frac{Q_{store}}{P_{loss}} = \frac{\nu_{pqm}}{\Delta\nu_{pqm}} \tag{1.11}$$

where the stored photon energy $Q_{store} = n_p h\nu$ for n_p photons, each with energy $h\nu$, and the power loss $P_{loss} = Q_{store}/\tau_p$ for a photon lifetime τ_p in the cavity. This gives a cavity quality $Q_c = 2\pi\nu\tau_p$ with a photon lifetime that depends on the internal cavity losses α_{int} (due to internal absorption and diffraction) and coupling losses α_m (i.e., output power through the cavity mirrors). The photon lifetime is given as

$$\tau_p = \frac{1}{v_g}\cdot\frac{1}{\alpha_{int}+\alpha_m} \qquad [\text{sec}] \tag{1.12}$$

for a pulse traveling with a group velocity v_g. If the power reflectivity of each mirror is R_{pi} and the internal losses are small, then the round-trip power-conservation condition [i.e., $R_{p1}R_{p2}\exp(2gL) = 1$] shows that the mirror loss that must be compensated by the gain g at threshold is

$$\alpha_m = -\frac{1}{2L}\ln(R_{p1}R_{p2}) \qquad [1/\text{cm}] \tag{1.13}$$

For example, if the laser cavity length $L = 100$ mm and the power reflectivity $R_{p1} = R_{p2} = 0.98$ for each mirror, then $\alpha_m \approx 0.002$/cm. Increasing the cavity length allows photons more time to travel around the cavity before being "expelled" by the mirror as output power, thus decreasing the mirror loss on a per-centimeter basis.

Physically, a low-loss cavity with high-reflectivity mirrors has a long photon lifetime and thus efficiently stores energy (i.e., has a large Q_c), while a high-loss cavity with low-reflectivity mirrors has a short photon lifetime and thus dissipates (or damps) energy (i.e., has a small Q_c). A typical gas-laser cavity has a Q_c value of $\approx 10^8$–10^9, indicating an extremely long photon lifetime: $\tau_p = Q_c/2\pi\nu \approx 0.025$–$0.250$ μsec for visible-wavelength light.

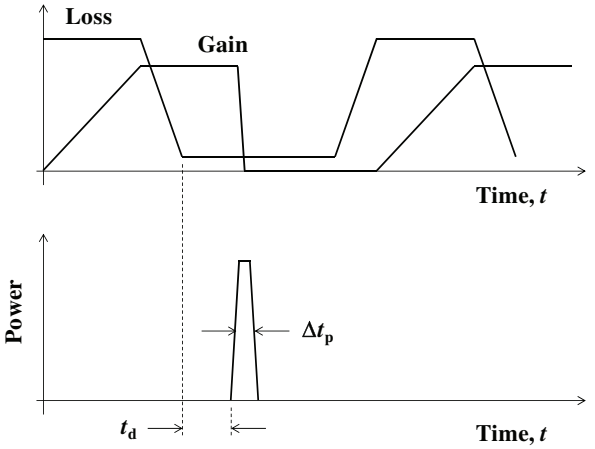

Figure 1.17 Q-switching is based on a buildup of gain when the cavity loss is high and a quick release of this energy in the form of a short pulse with $\Delta t_p \approx 1$–10 nsec when the loss is removed.

Q-switching, then, changes the laser cavity's losses to create shorter pulses than can be obtained with gain switching. By initially keeping the loss high (low Q_c) while the pump is activated, the population inversion and gain build up (Fig. 1.17); lasing is not possible, however, as the cavity loss from the switch is kept too high for the gain to overcome.

When the switch is turned off, the losses decrease (high Q_c) and the gain is then much higher than the total cavity loss; after a slight delay t_d, this gain is quickly utilized to create photons in the form of a short pulse with a FWHM width Δt_p. The Q-switch is then turned back on to increase the cavity loss again; if this did not happen, no additional pulses would be generated, and lasing would start at a steady-state power where gain balances losses.

Both active and passive technologies are available for Q-switching. Active switching typically uses an acousto-optic (AO) modulator to reduce the laser's internal losses in synchronization with the pulse's round-trip through the laser cavity, producing pulse widths on the order of 1–10 nsec.[17,18] Unfortunately, the AO modulator, while allowing large pulse energies and a variable switching rate, has a number of size, weight, and speed disadvantages in comparison with passive Q-switching.

Passive Q-switching with a *saturable absorber* generally produces lower-energy pulses but at a higher rate than an AO modulator. That is, just as the population inversion $N_2 - N_1$ in Fig. 1.9 can saturate to zero at a sufficiently high power, so can the absorption that is proportional to its negative (or $N_1 - N_2$). A saturable absorber thus has *less* loss—i.e., is "bleached"—as the incident power increases; the absorption at high power decreases as the number of atoms in a higher energy state approaches that in the lower, and the absorption (low-to-high energy transitions) approaches the emission

(high-to-low energy transitions). In this way, even a slight increase in peak pulse power reduces the loss of a saturable absorber, with the pulse Q-switching itself into narrower pulses in a self-reinforcing feedback loop with multiple round-trips through the laser cavity.

Typical materials with large saturable absorption include Cr^{4+}:YAG crystals for use at $\lambda \approx 1064$ nm,[19] semiconductor saturable-absorber mirrors (SESAMs) such as GaAs-InGaAs multilayers for $\lambda = 1064$ nm, and the recent development of low-loss graphene for broadband Q-switching.[20] Passive Q-switching—with its lower size, weight, complexity, and cost—is preferred over active switching unless large pulse energies are required. For either type of switching, peak power on the order of $10^4\times$ larger than the average power ($P_{\text{peak}} \approx$ 10–100 MW) is common—though only for 1–10 nsec, so not nearly enough kilowatt hours to bring down the power grid (in most cases).

In practice, a number of non-ideal characteristics limit the laser systems engineer's use of Q-switching. For example, the fast change in gain can lead to multi-axial-mode lasing; the time between pulses (or *timing jitter*) for saturable absorbers changing due to the high spontaneous emission rate from the large gain; and the lifetime of the saturable absorber being limited due to the high power densities.

For shorter pulses than are possible with Q-switching, a method known as *mode locking* is widely used.[21] That is, the axial modes determined by the combination of cavity length and gain bandwidth (Fig. 1.13)—which normally lase independently of each other—are coherently added in time (in phase, or *constructively interfere*) to produce short pulses on the order of 10 psec or less. This can occur for both inhomogeneous and homogeneous broadening of the gain, as an inhomogeneous gain medium normally supports multiple axial modes, and the homogeneous medium does so as well under non-steady-state (i.e., pulsed) conditions.

The modes must be shifted in phase by exactly the right amount to ensure that they all have the same phase at the same time somewhere in the cavity [for example, at the output mirror where the mode peaks line up on the right-hand side (RHS) of Fig. 1.12]. Even though the relative phase of any mode with respect to another is not initially known, we can modulate the beam—either actively or passively—so that the relative phase "locks" into a fixed value.

To understand how this can be achieved, an oscillating sinewave that is amplitude-modulated (AM) has frequency sidebands—a well-known result from Fourier analysis.[22] The frequency shift from the sinewave frequency $\omega = 2\pi\nu$ (in units of radians/sec) is simply the modulation frequency Ω, giving AM frequencies of $\omega - \Omega$, ω, and $\omega + \Omega$.

If the sinewave frequency corresponds to a laser mode frequency $\omega_m = 2\pi\nu_m$, and the modulation frequency $\Omega = 2\pi\Delta\nu = \pi c/nL$ equals the axial mode spacing $\Delta\omega_a$, then the AM sideband frequencies of $\omega - \Omega$ and $\omega + \Omega$ are superimposed on the neighboring axial modes ω_{m-1} and ω_{m+1}. If all

of the axial modes that are lasing are modulated at Ω, then all modes will be coupled to their neighbors, to their neighbor's neighbors, and so on. To the degree that Ω is constant, the modes are thus locked together—in frequency difference and in phase.[23]

Once locked, the modes coherently add together to produce pulses that are much shorter than implied by the amplitude-modulation frequency Ω (Fig. 1.18). With the peaks of N modes coinciding, for example, the sum from all modes increases the peak power by a factor of N if the power from each mode is the same, which is not the case given the dropoff in the gain curve, but is useful for understanding the concept of axial-mode addition.

In addition, Fig. 1.18 shows that the sum of in-phase axial modes also narrows the FWHM pulse width by a factor of N. This is analogous to a diffraction grating, where the beam reflected from the grating lines constructively interfere at a particular direction in space, with the width of the interference pattern decreasing as more lines are illuminated. The net effect of more modes, then, is to increase the peak power by a factor of N^2—one factor of N from power addition and one factor of N from pulse narrowing.

Given that the locking of more modes decreases the pulse width Δt_p, and a wider gain bandwidth $\Delta\nu_g$ allows more modes to have enough gain to lase, the pulse width is approximately

$$\Delta t_p = \frac{1}{N} \cdot \frac{2nL}{c} \approx \frac{1}{\Delta\nu_g} \qquad [\text{sec}] \tag{1.14}$$

for $N \approx \Delta\nu_g/\Delta\nu_a$ and $\Delta\nu_a = c/2nL$. Titanium-doped sapphire (or Ti:Al_2O_3) lasers, for example, have an extremely large gain bandwidth ($\Delta\lambda_g \approx 300$ nm) and are thus commonly used for generating pulses as short as 10 fsec.

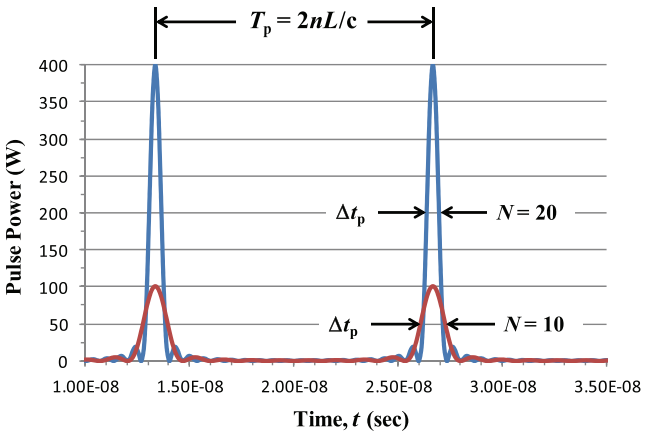

Figure 1.18 Mode-locked period T_p and FWHM pulse width Δt_p for $N = 10$ and $N = 20$ axial modes with equal power in each mode.

Finally, the pulse period $T_p = 2nL/c$ equals the round-trip time of a pulse as it circulates around the laser cavity. While the axial-mode picture in Fig. 1.12 appears to be static, the dynamic picture is that each mode reflects from the output mirror and coherently combines as an in-phase pulse after each round-trip transit $2L$ through the cavity, after which it is partially transmitted through the output mirror. Long fiber lasers, for example, have a long pulse period and relatively low pulse repetition frequency $\mathrm{PRF} = 1/T_p$, while much-shorter semiconductor lasers can in principle produce pulses at gigahertz rates.

As with Q-switching, both active and passive technologies are available for mode locking. Active mode locking typically uses a Pockels-cell electro-optic (EO) modulator[24] to create AM (or possibly frequency-modulated) sideband frequencies such that all of the axial modes that are lasing are modulated at Ω. Alternatively, we can think of the modulator as reducing the laser's internal losses in synchronization with the pulse's round-trip through the laser cavity, producing pulse widths on the order of 10 psec.[17]

Passive mode locking with a saturable absorber—using materials such as SESAMs—produces even shorter pulses. The power-dependent absorption modulates the beam power, creating frequency sidebands for each mode that are locked to the other modes. Alternatively, by transmitting the peak power while absorbing the leading and trailing edges of the pulse, saturable absorption narrows the pulse width; the process is ultimately limited by the gain bandwidth and, with much more hardware complexity than is described here, leads to pulses on the order of 10 fsec to 10 psec. As with Q-switching, passive mode locking is generally preferred to active mode locking with its increase in size, weight, complexity, and cost.

Typical examples of mode-locked USP applications include Ti:Al_2O_3 (also known as Ti:sapphire) lasers for research into molecular dynamics, and fiber lasers for "cold" laser machining to reduce thermal damage. This is an active area of product development and there are, of course, many engineering details required to implement mode locking. Practical limitations include variations in EO modulation frequency Ω, refractive-index variations across the gain bandwidth that modify the mode spacing, thermal expansion causing changes in cavity length and mode spacing, etc. For more details, see Paschotta[18] and Chapter 2.

1.2.4 Wavelength conversion

It sometimes happens that the inherent laser wavelength—1064 nm for a neodymium (Nd)-doped yttrium-orthovanadate (YVO_4) crystal as a gain medium, for example—is not useful for the task. In these cases, the laser designer must provide some mechanism of wavelength conversion, where the laser wavelength based on the gain medium is converted to some other wavelength of interest to meet the system requirements.

A common example is the conversion of 1064-nm light to 532 nm—a wavelength that the human eye can detect. Such conversion has been used for many years in low-cost laser pointers (Fig. 1.19), where the green (532-nm) light is easily obtained using a potassium titanium-oxide phosphate (KTP) crystal.[25] Another example is the conversion of 1064-nm light to 1570 nm; this conversion is useful because the 1570-nm photons are not as damaging to the eye as the 1064-nm photons, allowing the development of eye-"safer" laser rangefinders.

Figure 1.19 illustrates the wavelength-conversion hardware for second-harmonic generation (SHG). That is, by sending 1064-nm light of a sufficiently high peak power density (W/m^2) through a KTP crystal, second-harmonic wavelengths (one-half of 1064-nm) are generated. This occurs because the crystal's electrons cannot respond linearly to the large EM field; instead, an incident sinusoidal wave is re-emitted as a distorted waveform, which Fourier analysis tells us requires wavelengths shorter than the fundamental sinusoid—i.e., "harmonics"—to create. These harmonic wavelengths are in fact generated by the crystal, and the nonlinear conversion process of SHG is also known as *frequency doubling*.[26]

Another example of wavelength conversion is the use of an optical parametric oscillator (OPO) to create eye-"safer" photons at $\lambda = 1570$ nm

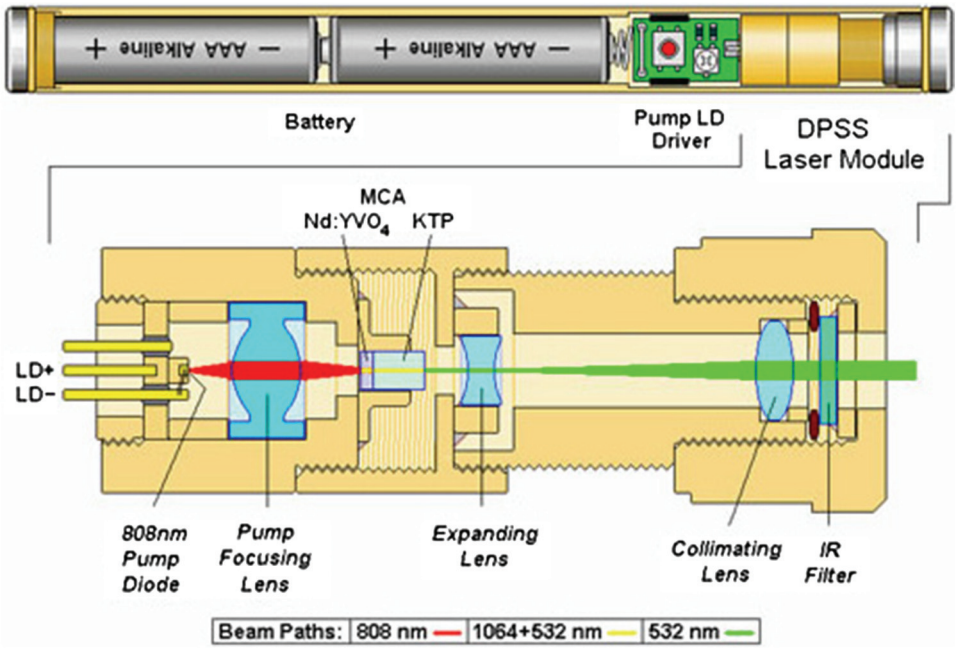

Figure 1.19 Second-harmonic generation (SHG) of 1064-nm photons from a Nd:YVO_4 laser into 532-nm photons uses a nonlinear crystal such as KTP. (Credit: Chris Chen, Wikimedia Commons.) (See color plate.)

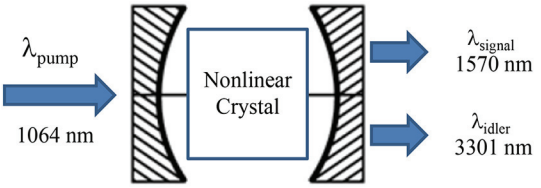

Figure 1.20 A high-energy photon at λ_{pump} = 1064 nm is converted to two lower-energy (longer-wavelength) photons by a nonlinear crystal such as KTP in a resonant cavity.

(Fig. 1.20). In this case, KTP (or some other nonlinear crystal) is used in a resonant cavity, thus assuring high-power density—for a nonlinear wavelength-conversion mechanism known as sum-frequency generation (SFG).

This nonlinear wavelength-conversion process relies on the conservation of photon energy to convert one short-wavelength (higher-energy) photon into two longer-wavelength (lower-energy) photons. With $E_{pump} = E_{signal} + E_{idler} = h\nu_{pump} = hc/\lambda_{pump}$ [from Eq. (1.1)], we have

$$\frac{1}{\lambda_{pump}} = \frac{1}{\lambda_{signal}} + \frac{1}{\lambda_{idler}} \qquad [1/\text{nm}] \tag{1.15}$$

where the sum of photon energies [or the sum of frequencies using Eq. (1.2)] gives this nonlinear mechanism its name. The labeling of a photon as a "signal" or "idler" is a bit arbitrary, as there are also applications where the MWIR 3301-nm wavelength shown in Fig. 1.20 is the desired output and is therefore the signal in that case.

In addition to SHG and SFG, there are a number of other nonlinear mechanisms used for wavelength conversion: frequency tripling or third-harmonic generation (THG), frequency quadrupling or fourth-harmonic generation (FHG), difference-frequency generation (DFG), etc.[26] To implement these technologies, the laser designer must consider wavelength range, nonlinear response, phase matching, temperature sensitivity, angular sensitivity, walk-off angle, and laser damage threshold, among other parameters.

In practice, two requirements play a key role for the laser systems engineer in the use of wavelength-conversion technologies:

- Conversion efficiency: Energy is lost in the conversion of wavelengths, and the conversion efficiency is the transmitted energy in comparison with the incident energy. The large peak power from pulsed lasers is more efficient at generating nonlinear effects than CW lasers. Up to 80% efficiency has been obtained for SHG using a KTP crystal at $\lambda = 1064$ nm, and >65% efficiency has been obtained for SHG with a lithium triborate (LBO) nonlinear crystal at $\lambda = 1064$ nm and $\Delta t_p \sim 2$ nsec.[27]
- Temperature tuning: The requirements on the laser pointer in Fig. 1.19 are not difficult to meet, while the power stability (Section 2.1.8) and

frequency stability (Section 2.1.9) requirements for a complex laser radar system that uses both 1064-nm and 532-nm photons to obtain information on the Earth's atmosphere from a low-Earth orbit may be extremely challenging. In such cases, temperature tuning of the nonlinear crystal—i.e., controlling the refractive indices $n(\nu)$ and $n(2\nu)$ to maintain phase matching—may be required; see Ref. 27 for more details.

Summarizing Section 1.2, laser designers must control a number of important parameters, including: (1) axial modes for "color" purity and temporal coherence, (2) transverse modes for directionality and spatial coherence, (3) pulse width and period, and (4) wavelength conversion. Many more engineering specifications of importance to the user of lasers—i.e., the laser systems engineer—will be reviewed in Chapter 2. A brief overview of the laser systems engineering process and the remainder of the book are first given in Section 1.3.

1.3 Laser Systems Engineering

An awareness of the laser designer's options will only simplify the laser systems engineer's job, as many of the tasks are similar. But even with this understanding, an obvious first question to ask for any system architecture is: why—or under what conditions—is a laser even necessary? While we have reviewed some of the properties of lasers, answering a question such as this requires a follow-on question: What are the properties of the alternatives?

The alternatives to lasers are incoherent sources—solar energy, arc lamps, tungsten-halogen bulbs, and so on[28]—and the first comparison (or design trade) to make is how much power is available from each type of source. This may seem like a strange design trade; after all, if the laser and the incoherent source both emit 100 mW of power, then isn't 100 mW available from both for material ablation, biomedical sample fluorescence, or any other application?

Figure 1.21 illustrates why this is not the case. In Fig. 1.21(a), we see that an incoherent source on the left of the lens is imaged to something resembling the source with a magnification $m_{\text{lens}} = -s_i/s_o$ for an object distance s_o and an image distance s_i. In Fig. 1.21(b), on the other hand, a laser of the same size and placed at the same object distance s_o is imaged to a focused spot whose size depends on the laser wavelength λ, the lens diameter D, and the beam quality M^2.

The reason for the difference in Fig. 1.21 is that the wavefronts from the incoherent source are emitted by each point on the source independently of the other (Fig. 1.8), and thus recombine to an image independently of each other as well. Each point on the source is in fact focused to a small spot, but

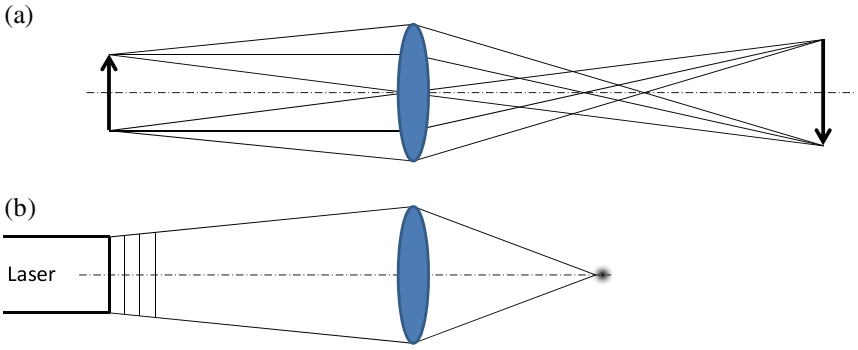

Figure 1.21 (a) A lens reproduces a nearby incoherent source into an image resembling the source. (b) A lens images a nearby laser beam of the same size into a small focused spot.

because each point emits independently of the others—i.e., incoherently—they recombine as shown on the RHS of Fig. 1.21(a).

For the laser, however, the points are to a large degree emitting in phase, and thus coherently recombine into a small, focused spot. The degree to which they are in phase depends on the spatial coherence, which as we will see in Chapter 3 determines in part the size of the spot.

In addition, essentially all of the power emitted by the laser is collected by the lens, while a large fraction of the power emitted by the incoherent source is not. That is, the laser's full-divergence angle (or directionality) $2\theta_o \approx \lambda/D$, while an incoherent source typically emits at least some power into a sphere encompassing the source. Sizing a lens to capture the laser's divergence angle is thus relatively straightforward (see Chapter 6), while specialized reflectors are required to capture even a decent fraction of an incoherent source's power.

Finally, the incoherent source emits an extremely large wavelength band, while the laser typically does not (exceptions such as super-continuum lasers will be reviewed in Section 2.2.3).

It turns out that it is possible to use an incoherent source in such a way that it has many of the properties of lasers—but at a cost. Figure 1.22 illustrates how this is possible using a small aperture size s (such as a pinhole after the source itself) and a narrow bandpass filter (BPF) to transmit only a small fraction of the wavelengths emitted. In addition, if the pinhole is placed

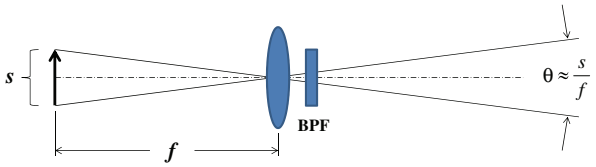

Figure 1.22 An incoherent source can be designed with a small aperture size s to increase spatial coherence, and a bandpass filter (BPF) to control temporal coherence.

at the focal length of the lens, the lens collimates the incoherent source with a divergence angle $\theta \approx s/f$.[28] As the pinhole is made smaller—and the wavefront across it is thus more coherent—the divergence angle will approach the full divergence angle $2\theta_o$ of a laser, after which θ is limited by wavefront diffraction and cannot be made any smaller (see Problem 1.10).

So with some additional optics, it is possible to design an incoherent source with a spatial and temporal coherence similar to a laser's—but at the cost of a huge loss of power. The pinhole, for example, allows only a small fraction of the incoherent source's light through it, as does the BPF. One of the unique features of a typical laser, then, is not the directionality and narrow wavelength band, but these properties *combined with* almost all of its output power available for useful tasks such as material ablation, fluorescence microscopy, or directed energy.

For a laser *system*, however, laser output power is not the whole story, and there are other requirements, components, and subsystems that must be considered as well. The perspective taken to do this—that of the laser systems engineer—is sometimes thought of as "designing the right laser" versus "designing the laser right." Unfortunately, this is both incomplete and overly centered on the laser designer's goal of designing the laser right. Designing the right laser—i.e., one that meets system-level requirements such as output power—is certainly key, but designing the right optical, scanning, and detector subsystems is equally critical.

Table 1.4 is a common systems-engineering tool that illustrates one way in which these other subsystems are taken into account. Known as a trade table, it compares three different design options for a laser radar system. The options evaluated in this case—and there are many other criteria that must also be used—are based on a power budget, i.e., is there enough power reflected from the target to be "useful" to the detector?

In this simple example, system performance depends on three components: the laser output power, the size of the telescope aperture collecting the reflected power, and the detector's sensitivity (i.e., the smallest power it can detect). In Design 1, it was assumed by the laser-system architect that a laser with 1 W of output power was available, as well as a telescope aperture of 100 mm and a minimum power for the detector (or *sensitivity*) of 1 nW.

Table 1.4 A trade table summarizing component specifications for laser radar system design options.

Component	Design 1	Design 2	Design 3
Laser Power	1 W	0.1 W	0.1 W
Telescope Aperture	100 mm	316 mm	100 mm
Detector Sensitivity	1 nW	1 nW	0.1 nW

In reviewing the architecture with the laser designer, however, it was found that the 1-W laser would not be ready for product development for quite a while, and that a 100-mW laser was the only reliable option for now.

So with a factor of $10\times$ less power available from the laser, a factor of $10\times$ increase in telescope area (Design 2)—or a $10^{1/2} = 3.16\times$ increase in aperture size—was considered to compensate. At this point, the optical engineer on the project mentioned that such an aperture was much larger in terms of size and weight than the customer would consider, thus removing Design 2 as one of the options.

Fortunately, in reviewing the architecture with the detector specialist, it was found that detectors with $1/10^{th}$ the sensitivity were available as commercial off-the-shelf (COTS) parts, thus allowing Design 3 to proceed as the baseline architecture.

As we will see in Chapter 6, there are a number of additional details such as beam quality to consider when developing power budgets, and this simple example illustrates only one of the many design trades between the subsystems—laser, optics, scanning, and detector—to be reviewed in this book. Included are chapters on laser types and selection (Chapter 2), the unique requirements on using optical components in laser systems (Chapter 4), scanning technologies and system trades (Chapter 5), and detector types and selection (Chapter 7). Interspersed between these chapters are the concepts needed to understand beam propagation (Chapter 3) and radiometry (Chapter 6). The book does not include software or electrical[29] subsystems.

The emphasis in all chapters is on real-world design problems and the first-order equations and COTS components used to solve them. As with any book, not every topic can be included; however, readers may also find my previous books useful for understanding the many differences between laser systems and conventional optical systems using incoherent sources [*Optical Systems Engineering*, McGraw-Hill (2011)], or obtaining additional details on the optomechanical aspects of building laser systems [*Optomechanical Systems Engineering*, John Wiley (2015)].

1.4 Problems

1.1 Analyze the 1950s Laser-Eyed Monster from the perspective of the laser systems engineer. For example, is there a possible eye-safety issue associated with launching a high-power beam through one's eyes? In addition, how would such a laser be powered, how would the heat be removed, and how would the wavelength be controlled? Hint: See Chapter 2 for additional considerations.

1.2 What is the linewidth $\Delta\lambda$ for an inhomogeneously broadened laser that lases at five axial-mode frequencies based on Eq. (1.6)?

1.3 Does the transmission of an etalon drop off faster or slower with laser frequency as the etalon reflectivity R is increased? Are there disadvantages to using a higher reflectivity?

1.4 What is the cold-cavity (zero gain) FWHM bandwidth $\Delta\nu_{SLM}$ of the individual longitudinal modes of a laser resonator based on the mirror reflectivities? (Hint: What is the finesse of the laser cavity?) And is this result consistent with that obtained from Eqs. (1.11), (1.12), and (1.13)?

1.5 What is the axial mode spacing $\Delta\nu_a$ for the confocal cavity? How does it compare with that of the planar-mirror cavity?

1.6 Are there any laser cavity designs that have the same absolute value of the axial-mode frequency as the planar-mirror cavity? Hint: See Ref. 9.

1.7 What is the approximate cavity length L needed to obtain the mode-locked pulse period T_p shown In Fig. 1.18? The gain medium's refractive index $n \approx 1$.

1.8 In a mode-locked laser, what is the relation between the coherence length d_c and the pulse width Δt_p?

1.9 If a SFG oscillator creates one 2128-nm photon from 1064-nm photons, what is the wavelength of the second long-wavelength photon that an OPO must produce to conserve energy?

1.10 Referring to Fig. 1.22, what pinhole size is required to give the same collimated-beam full-divergence angle as a laser with $2\theta_o = 4\lambda/\pi D$? Assume that the wavelength $\lambda = 1$ μm and the smallest relative aperture available for the lens is $f/D \equiv f/\# = 1$.

Notes and References

1. See, for example, A. Samman, L. Rimau, J. R. McBride, R. O. Carter, W. H. Weber, C. Gmachl, F. Capasso, A. L. Hutchinson, D. L. Sivco, and A. Y. Cho, "Potential use of near, mid, and far infrared laser diodes in automotive LIDAR applications," *IEEE Vehicular Technology Conference*, pp. 2084–2089 (2000); or R. Halterman and M. Bruch, "Velodyne HDL-64E lidar for unmanned surface vehicle obstacle detection," *Proc. SPIE* **7692**, 76920D (2010) [doi: 10.1117/12.850611].

2. S. W. Hell, "Nanoscopy with focused light," *Proc. SPIE* **8882**, 888203 (2013) [doi: 10.1117/2032261].

3. G. P. Agrawal, *Fiber-Optic Communication Systems*, Fourth Edition, John Wiley & Sons (2010).

4. J. König and T. Bauer, "Fundamentals and industrial applications of ultrashort pulsed lasers at Bosch," *Proc. SPIE* **7925**, 792510 (2011) [doi: 10.1117/12.878593].

5. K. V. Chellappan, E. Erden, and H. Urey, "Laser-based displays: A review," *Applied Optics* **49**(25), F79–F98 (2010).

6. P. Lubin, G. B. Hughes, J. Bible, J. Bublitz, J. Arriola, C. Motto, J. Suen, I. Johansson, J. Riley, N. Sarvian, D. Clayton-Warwick, J. Wu, A. Milich, M. Oleson, M. Pryor, P. Krogen, M. Kangas, and H. O'Neill, "Toward directed energy planetary defense," *Optical Engineering* **53**(2), 025103 (2014).

7. See, for example, Salvador Dali, "The Laser Unicorn Disintegrates the Horns of the Cosmic Rhinoceros," 1974.

8. E. P. Goodwin and J. C. Wyant, *Field Guide to Interferometric Optical Testing*, SPIE Press, Bellingham, Washington (2006) [doi: 10.1117/3.702897].

9. A. E. Siegman, *Lasers*, University Science Books, Sausalito, California (1986).

10. H. Weichel, "Lasers" in *The Infrared & Electro-Optical Systems Handbook* Vol. **3**, W. D. Rogatto, Editor, ERIM, Ann Arbor, Michigan and SPIE Press, Bellingham, Washington, Chapter 10 (1993).

11. In practice, small time-varying fluctuations in cavity spacing, lattice strain, and the refractive index of the gain medium lead to *mode hops*; see Section 2.1.9 for more details.

12. A. Mooradian, "Laser linewidth," *Physics Today* **38**(5), 42–50 (1985).

13. See, for example, R. Hauck, H. P. Kortz, and H. Weber, "Misalignment sensitivity of optical resonators," *Applied Optics* **19**(4), 598–601 (1980); or Ref. 9, Section 19.4.

14. This section does not apply to lasers that rely on total-internal-reflection (TIR) waveguiding between the mirrors, with semiconductor and fiber lasers being the most common. For those lasers that do not rely on waveguides, i.e., solid-state and gas lasers, the free-space modes in this section are applicable; see Ref. 15 for more information on waveguide modes.

15. C. R. Pollock, *Fundamentals of Optoelectronics*, Richard D. Irwin Publishing, Homewood, Illinois (1994).

16. Spatial coherence is defined by correlations across the wavefront (stationary phase). Unfortunately, this leaves open the possibility that

a wavefront with phase errors (a single TEM_{01} mode, for example) is spatially coherent. As we will see in detail in Chapter 3, the concept of beam quality avoids this limitation by using a comparison of a wavefront not with itself, but with an ideal (uniphase), diffraction-limited ($M^2 = 1$) TEM_{00} mode with zero phase errors across it, and which can be focused to the smallest-possible spot size.

17. R. Paschotta, *Field Guide to Lasers*, SPIE Press, Bellingham, Washington (2008) [doi: 10.1117/3.767474].

18. R. Paschotta, *Field Guide to Laser Pulse Generation*, SPIE Press, Bellingham, Washington (2008) [doi: 10.1117/3.800629].

19. J. Zheng, S. Zhao, and L. Chen, "Laser-diode end-pumped passively Q-switched intracavity doubling Nd:YVO_4KTP laser with Cr^{4+}:YAG saturable absorber," *Opt. Eng.* **41**(8), 1970–1975 (2002) [doi: 10.1117/1.1486245].

20. Z. Zheng, C. Zhao, S. Lu, Y. Chen, Y. Li, H. Zhang, and S. Wen, "Microwave and optical saturable absorption in graphene," *Optics Express* **20**(21), 23201–23214 (2012).

21. H. A. Haus, "Mode-locking of lasers," *IEEE Journal on Selected Topics in Quantum Electronics* **6**(6), 1173–1185 (2000).

22. J. F. James, *A Student's Guide to Fourier Transforms*, Cambridge University Press, Cambridge (1995).

23. C. C. Cutler, "Why does linear phase shift cause mode locking?" *IEEE Journal of Quantum Electronics* **28**(1), 282–288 (1992).

24. V. V. Matylitsky, F. Hendricks, and J. Aus der Au, "Femtosecond laser ablation properties of transparent materials: Impact of the laser process parameters on the machining throughput," *Proc. SPIE* **8611**, 861112 (2013) [doi: 10.1117/12.2003691].

25. Such lasers can also present a hazard to the eye due to leakage of 1064-nm light. For more details, see J. Galang, A. Restelli, E. W. Hagley, and C. W. Clark, "A red light for green laser pointers," *Optics and Photonics News*, pp. 11–13, Oct. 2010.

26. R. W. Boyd, *Nonlinear Optics*, Third Edition, Academic Press, San Diego (2008).

27. N. W. Sawruk, P. M. Burns, R. E. Edwards, T. Wysocki, A. Van Tujil, V. Litvinocitch, E. Sullivan, and F. E. Hovis, "ICESat-2 laser technology readiness level evolution," *Proc. SPIE* **9342**, 93420L (2015) [doi: 10.1117/12.2080531].

28. K. J. Kasunic, *Optical Systems Engineering*, McGraw-Hill, New York (2011).

29. P. C. D. Hobbs, *Building Electro-Optical Systems*, Second Edition, John Wiley & Sons, Hoboken, New Jersey (2009).

Glossary of Symbols and Acronyms

A	area (m^2); optical absorption
A_b	beam area (mm^2)
A_d	detector area (mm^2)
A_{EP}	entrance pupil area (mm^2)
A_o	illuminated object area (mm^2)
A_p	pixel area (μm^2)
AO	acousto-optic
AOI	angle of incidence (rads)
APD	avalanche photodiode
APS	active-pixel sensor
AR	antireflection
ASE	amplified spontaneous emission
$A\Omega$	étendue (m^2-sr)
B	focused blur diameter (μm); PSD frequency exponent
B_{SA}	focused blur diameter due to spherical aberration (μm)
BFD	back focal distance
BPF	bandpass filter
BPP	beam-parameter product (mm-mrad)
BSDF	bidirectional scatter distribution function
c	speed of light, $\approx 3 \times 10^8$ m/sec
C	wavefront or surface curvature (1/mm)
C_o	wavefront curvature incident on lens (1/mm)
C_i	wavefront curvature exiting lens (1/mm); image contrast
C_{sp}	speckle contrast
C_{well}	charge-well capacitance (pF)
CA	clear aperture
CCD	charge-coupled device
CDS	correlated double sampling
CMOS	complementary metal-oxide semiconductor

CoO	cost of ownership
COTS	commercial off-the-shelf
cps	counts per second
CRT	cathode-ray tube
CTE	charge-transfer efficiency; coefficient of thermal expansion
CTIA	capacitive transimpedance amplifier
CW	continuous wave
d	distance (m)
d_c	coherence length (m)
$d_{c,n}$	coherence length in a medium of index n (m)
d_{FP}	Fabry–Pérot cavity thickness (mm)
dn/dT	change in index with temperature (1/K)
d_p	pixel size (μm)
D	lens diameter or aperture size (mm); fiber diameter (μm)
D_{1/e^2}	beam diameter ($1/e^2$) incident on or exiting from a lens (mm)
$D_b(z)$	beam diameter (mm)
D_{EP}	entrance-pupil diameter (mm)
D_o	waist diameter (mm)
DBR	distributed Bragg reflector
DCR	dark-count rate [e^-/sec or counts per sec (cps)]
DE	directed energy
DFG	difference-frequency generation
DI	direct injection
DLC	diamond-like carbon
DoF	degrees of freedom
DOF	depth of focus (μm)
dpi	dots per inch
DPSS	diode-pumped solid-state
DWDM	dense wavelength-division multiplexing
E	irradiance (W/m^2); Young's modulus (GPa)
E_g	bandgap energy (J or eV)
E_i	electron energy for energy level i (J or eV)
E_o	Gaussian peak irradiance (W/m^2)
E_p	photon energy (J or eV)
EB-CCD	electron-bombarded CCD
EB-CMOS	electron-bombarded CMOS
EFL	effective focal length (mm)
EM	electromagnetic
EM-CCD	electron-multiplying CCD
EOL	end of life

EOM	electro-optic modulator
ESD	energy spectral density
f	focal length (mm); electrical frequency (Hz)
f_d	FPA cutoff frequency (lp/mm)
f_{RO}	relaxation-oscillation frequency (Hz)
f_s	spatial frequency (lp/mm); mirror scan frequency (Hz)
$f/\#$	relative aperture, $\equiv f/D$
F	fluence (J/m^2)
$F(G)$	excess noise factor
F_R	cavity finesse based on power reflectivity R_P
FBG	fiber Bragg grating
FET	field effect transistor
FF	FPA fill factor
FHG	fourth-harmonic generation
FOI	field of illumination (rad)
FOR	field of regard (rad)
FOV	field of view (rad)
FP	Fabry–Pérot
FPA	focal plane array
FPN	fixed-pattern noise
FR	frame rate [Hz or frames per sec (fps)]
FSM	fast-steering mirror
FSR	free spectral range (Hz)
FWHM	full-width at half-maximum
g	laser gain (1/cm)
g_i	laser-cavity stability parameter
G	detector gain; thermo-optic constant (1/K)
GM-APD	Geiger-mode APD
GVD	group-velocity dispersion
h	Planck's constant, $= 6.626 \times 10^{-34}$ J-sec; mirror thickness (mm)
HFOV	half-FOV (rad)
HAZ	heat-affected zone
HPD	hybrid photodetector
HR	high reflectivity
HSF	high spatial frequency
HT	high transmission
HWP	half-wave plate
i	current (A)
i_b	detector background current (A)

i_d	detector current (A)
i_{dc}	detector dark current (A)
i_s	detector signal current (A)
i_{th}	laser threshold current (A)
I	intensity (W/sr)
IAD	ion-assisted deposition
IBS	ion-beam sputtering
ICCD	intensified CCD
IFOV	instantaneous FOV (μrad)
IR	infrared
IRCM	IR countermeasure
ISO	International Standards Organization
J	rotational moment of inertia (kg-m^2)
k	APD ionization coefficient; thermal conductivity (W/m-K)
K_{SA}	blur size factor due to spherical aberration
K_T	truncation factor
KTP	potassium titanium-oxide phosphate
L	length (m); radiance or brightness (W/m^2-sr)
L_i	image radiance (W/m^2-sr)
L_s	source radiance (W/m^2-sr)
L_λ	spectral radiance or brightness (W/m^2-sr-nm)
LAM	laser additive manufacturing
LCOS	liquid crystal on silicon
LCPG	liquid crystal polarization grating
LDT	laser damage threshold (J/cm^2 or W/cm^2)
LED	light-emitting diode
LIDT	laser-induced damage threshold
LLL	low light level
LMA	large mode area
LM-APD	linear-mode APD
lp	line pair
LWIR	longwave IR
m	integer, 1, 2, 3…; waist magnification w_{02}/w_{01}; mass (kg)
m_i	image modulation; image magnification
m_{lens}	lens object-image magnification
m_p	peak waist magnification w_{02}/w_{01} at 1f:1f conjugates
M	square-root of M^2
M^2	beam quality compared with a diffraction-limited TEM$_{00}$ beam

M_a	afocal telescope magnification
MCP	micro-channel plate
MCT	mercury cadmium telluride
MEMS	micro-electromechanical system
MLM	multiple longitudinal mode
MMF	multimode fiber
MOPA	master-oscillator power amplifier
MPE	maximum permissible exposure; multiphoton excitation
MPN	mode-partition noise
MPPC	multipixel photon counter
MRF	magneto-rheological finishing
MSF	mid-spatial-frequency
MTF	modulation transfer function
MTF_{det}	detector MTF
MTF_{opt}	optical MTF
MTF_{sys}	system MTF
MTTF	mean time-to-failure
MWIR	midwave IR
n	refractive index
n_e	number of electrons
n_f	number of polygon facets
n_p	number of photons
n_s	number of signal electrons
n_w	well depth (e^-)
$n_{\sigma amp}$	number of amplifier noise electrons (e^-)
$n_{\sigma b}$	number of background noise electrons (e^-)
$n_{\sigma dc}$	number of dark-current noise electrons (e^-)
$n_{\sigma FPN}$	number of spatial noise electrons (e^-)
$n_{\sigma read}$	number of read noise electrons (e^-)
$n_{\sigma RIN}$	number of RIN noise electrons (e^-)
$n_{\sigma s}$	number of signal noise electrons (e^-)
$n_{\sigma sp}$	number of speckle noise electrons (e^-)
N	number of longitudinal modes; resolvable spots; detector noise (A or e^-)
N_e	number of electrons per second (e^-/sec)
N_i	number of electrons per unit volume in energy level i ($1/m^3$)
N_p	number of photons per second (#/sec); number of pixels
NBF	narrow-band filter
NEP	noise-equivalent power (W or $W/Hz^{1/2}$)
NEP_{amp}	amplifier-limited NEP (W or $W/Hz^{1/2}$)
NEP_s	signal-limited NEP (W or $W/Hz^{1/2}$)

NEPh	noise-equivalent photons (# of photons)
NIR	near-IR
NPRO	nonplanar ring oscillator
NRE	nonrecurring engineering
NSD	noise spectral density ($A/Hz^{1/2}$)
NUC	non-uniformity correction
NUV	near UV
OCS	optical cross-section (m^2/sr)
OCT	optical coherence tomography
OPA	optical phased array
OPL	optical path length (= *nd*, μm or waves)
OPO	optical parametric oscillator
OPSL	optically pumped semiconductor laser
OXT	optical crosstalk
P	CW output power (W)
P_{avg}	average output power (W)
P_{elec}	electrical power (W)
P_d	probability of detection
P_{fa}	probability of false alarm
P_h	horizontally polarized power
P_{inc}	optical power incident on a lens or surface (W)
P_{peak}	peak output power (W)
P_r	optical power reflected by a lens or surface (W)
P_t	optical power transmitted by a lens or surface (W)
P_{th}	thermal heat load due to lens absorption (W)
P_v	vertically polarized power
PBS	polarizing beamsplitter
PCF	photonic crystal fiber
PDE	photon detection efficiency
PDH	Pound, Drever, and Hall
PER	polarization extinction ratio
PIB	power-in-bucket
PIN	*p-i-n* photodetector
PM	polarization-maintaining
PMT	photomultiplier tube
PRF	pulse repetition frequency (Hz)
PRNU	photo-response non-uniformity
PRR	pixel readout rate (Hz)
PSD	power spectral density (nm^2-m), aka energy spectral density
PV	peak to valley; photovoltaic
PZT	piezoelectric transducer

q	electron charge, $= 1.602 \times 10^{-19}$ C/e$^-$; lens shape factor
Q	heat load (W)
Q_c	cavity quality
Q_p	pulse energy (J)
Q_{store}	cavity photon-energy storage (J)
QCL	quantum-cascade laser
QCW	quasi-continuous wave
QE	quantum efficiency
QWP	quarter-wave plate
r	radial coordinate (m)
R	average power reflectivity; diffraction ripple; range (m)
$R(z)$	Gaussian wavefront radius of curvature (mm)
R_f	Fresnel surface reflectivity
R_g	responsivity after including detector gain G (A/W)
R_i	wavefront radius of curvature exiting lens (mm)
R_o	wavefront radius of curvature incident on lens (mm); detector responsivity (A/W)
R_p	reflectance of p-polarized light
R_{pi}	power reflectivity of surface i
R_s	reflectance of s-polarized light
R_t	thermal resistance (K/W)
RHS	right-hand side
RIN	relative intensity noise (1/Hz or dB/Hz)
RMS	root mean square
ROI	region-of-interest
ROIC	readout integrated circuit
RPM	revolutions per minute
RSS	root sum square
s	incoherent source size (mm)
s_o	object distance (mm)
s_i	image distance (mm)
sCMOS	scientific-grade CMOS
S	Strehl ratio; mirror width (mm); detector signal (A or e$^-$)
SA	spherical aberration
SAM	saturable-absorber mirror
SESAM	semiconductor saturable-absorber mirror
SFE	surface figure error (μm or waves)
SFG	sum-frequency generation
SHG	second-harmonic generation
SiPM	silicon photomultiplier
SLM	single longitudinal mode

SMF	single-mode fiber
SNR	signal-to-noise ratio
SPAD	single-photon avalanche detector
SPCM	single-photon counting module
SPDT	single-point diamond turning
SRS	stimulated Raman scattering
STED	stimulated emission depletion
SWaP	size, weight, and power
SWIR	shortwave IR
t	time (sec)
t_f	time of flight (sec)
t_{int}	detector integration time (sec)
t_s	scan time (sec)
T	truncation ratio; optical transmittance; temperature (K); torque (N-m)
T_{atm}	atmospheric transmission
T_{ext}	external transmission
T_{int}	internal transmission
T_{opt}	optical transmission
T_p	pulse period (sec)
T_{PIB}	transmitted power-in-bucket
T_{trunc}	optical transmission after truncation losses
TCK	transfer clock
TDL	times diffraction limited
TEA	transversely excited atmospheric
TEC	thermoelectric cooler
TEM_{pq}	transverse electro-magnetic mode with integer number of nodes p and q
THG	third-harmonic generation
TIA	transimpedance amplifier
TIR	total internal reflection
TIS	total integrated scatter
ToF	time of flight (sec)
ULE	ultralow expansion
USP	ultrashort pulse
UV	ultraviolet
v	scan velocity (m/sec)
v_g	group velocity (m/sec)
V	volume (cm^3)
V_b	bias voltage (V)

V_{br}	breakdown voltage (V)
VAC	volts of alternating current
VCSEL	vertical-cavity surface-emitting laser
VECSEL	vertical-external-cavity surface-emitting laser
VIS	visible
VPR	pixel reset voltage
VUV	vacuum UV
$w(z)$	Gaussian $1/e^2$ beam radius (mm)
w_o	Gaussian $1/e^2$ waist radius (mm)
w_{01}	Gaussian $1/e^2$ object-waist radius (mm)
w_{02}	Gaussian $1/e^2$ image-waist radius (mm)
w_{oM}	laser waist radius for an embedded beam with quality M^2 (mm)
WD	working distance
WFE	wavefront error (μm or waves)
WP	wall plug
x	transverse coordinate (m)
x_p	pixel pitch (μm)
y	transverse coordinate (m)
y_{MSF}	surface error (nm)
z	axial (or longitudinal) propagation axis (m)
z_1	object waist-to-lens distance (mm)
z_2	lens-to-image waist distance (mm)
z_{FF}	far-field distance (m)
z_R	Rayleigh range (m)
z_{R1}	Rayleigh range of the object waist (m)
z_{R2}	Rayleigh range of the image waist (m)
α	angular acceleration (rad/sec^2)
α_{int}	internal loss (1/cm)
α_m	mirror loss (1/cm)
$\alpha_m(\lambda)$	material attenuation coefficient (1/cm)
α_t	coefficient of thermal expansion (1/K)
β_{SA}	angular blur size due to spherical aberration (μrad)
δ	mirror dynamic deflection (μm)
δ_{RMS}	RMS surface finish (Å or nm)
δ_T	mirror thermal distortion (μm)

Δd	surface figure error (SFE) or irregularity (μm or waves)
Δf	electrical bandwidth (Hz)
ΔL	change in cavity length (μm)
ΔL_t	change in cavity length due to thermal expansion (μm)
ΔQ	gain bandwidth (J)
ΔR	range resolution (m)
Δt_p	pulse width (sec)
ΔT	temperature change (C or K)
Δv	velocity variation (m/sec)
Δx	distance between spatial features (mm)
Δy	change in beam-pointing location (μm)
Δz_{ast}	axial astigmatism (μm)
$\Delta\phi$	phase difference (rad)
$\Delta\lambda$	emission linewidth (μm or nm)
$\Delta\lambda_g$	gain bandwidth (μm or nm)
$\Delta\nu$	emission linewidth (Hz)
$\Delta\nu_a$	axial mode spacing (Hz)
$\Delta\nu_g$	gain bandwidth (Hz)
$\Delta\nu_L$	frequency shift or broadening due to change in cavity length (Hz)
$\Delta\nu_{MLM}$	multi-longitudinal-mode emission linewidth (Hz)
$\Delta\nu_R$	laser or etalon cold-cavity transmission bandwidth (Hz)
$\Delta\nu_{SLM}$	single-longitudinal-mode cold-cavity linewidth (Hz)
$\Delta\nu_{ST}$	Schawlow–Townes single-longitudinal-mode emission linewidth (Hz)
$\Delta\theta$	mirror misalignment angle or change in beam pointing angle (μrad)
$\Delta\theta_d$	diffraction angle
$\Delta\theta_m$	change in mirror mechanical pointing angle
$\Delta\omega$	linewidth (rad/sec)
$\Delta\omega_a$	axial mode spacing (rad/sec)
ε	obscuration ratio
Φ	optical power collected by an optical system (W)
Φ_L	refractive or reflective power of a lens or mirror (1/m)
γ_{obs}	obscuration loss
η	polygon geometric efficiency factor
η_{GM}	Geiger-mode avalanche efficiency
η_s	slope efficiency (W/A)
η_{QE}	quantum efficiency – also see QE
η_{WP}	wall-plug efficiency (%)

λ	wavelength (μm or nm)
λ_o	center wavelength (μm or nm)
ν	optical frequency (= c/λ, Hz)
ν_m	axial mode frequency (Hz)
ν_p	pump optical frequency (Hz)
ν_{pqm}	transverse mode frequency (Hz)
θ	angular coordinate or angular scan range (rad)
θ_{01}	far-field half-divergence angle incident on lens (rad)
θ_{02}	far-field half-divergence angle exiting lens (rad)
θ_d	diffraction angle (rad)
θ_{DL}	diffraction-limited full-divergence angle (rad)
θ_o	far-field half-divergence angle (rad)
θ_s	scatter angle (rad)
θ_{slow}	slow-axis full-divergence angle (rad)
$\dot{\theta}$	angular velocity (rad/sec)
$\ddot{\theta}$	angular acceleration (rad/sec^2)
ρ	power reflectivity; mass density (kg/m^3)
σ_{amp}	amplifier noise (A)
σ_{APD}	APD-detector signal noise (A)
σ_b	detector background noise (A)
σ_{dc}	detector dark-current noise (A)
σ_{FPN}	detector spatial noise (A)
σ_n	detector noise current (A)
σ_o	second-moment beam radius (mm)
σ_P	standard deviation of output power (W)
σ_{read}	detector read noise (A)
σ_{RIN}	detected RIN noise (A)
σ_s	detector signal noise (A)
σ_{sp}	detected speckle noise (A)
τ_c	coherence time (sec)
τ_p	photon lifetime or energy storage time (sec)
ω	optical frequency (= $2\pi\nu$, rad/sec)
Ω	modulation frequency (rad/sec); solid angle (sr)
$\Omega_{f/\#}$	solid angle of lens focusing cone (sr)
Ω_{IFOV}	solid angle of pixel IFOV (sr)

Index

Keith J. Kasunic has more than 30 years of experience developing optical, electro-optical, infrared, and laser systems. He holds a Ph.D. in Optical Sciences from the University of Arizona, an M.S. in Mechanical Engineering from Stanford University, and a B.S. in Mechanical Engineering from MIT. He has worked for or been a consultant to a number of organizations, including Lockheed Martin, Ball Aerospace, Sandia National Labs, and Nortel Networks; he is currently the Technical Director of Optical Systems Group, LLC. He is also the author of two textbooks [*Optical Systems Engineering* (McGraw-Hill, 2011) and *Optomechanical Systems Engineering* (John Wiley, 2015)], an Instructor for SPIE, an Affiliate Instructor with Georgia Tech's SENSIAC, and an Instructor for the Optical Engineering Certificate Program at Univ. of California – Irvine.